Theor Chem Acc (2010) 127:183–193
DOI 10.1007/s00214-009-0721-y

REGULAR ARTICLE

Temperature effects for vibrational relaxation of hydrogen adsorbed on Si(100): a stochastic multiconfigurational time-dependent Hartree (MCTDH) study

Franziska Lüder · Mathias Nest · Peter Saalfrank

Received: 25 September 2009 / Accepted: 15 December 2009 / Published online: 13 January 2010

Abstract Using a previously developed system–bath model Hamiltonian for the vibrational relaxation of H atoms adsorbed on a Si(100) surface (Andrianov and Saalfrank in J Chem Phys 124:034710, 2006), temperature effects on the relaxation of excited adsorbate vibrations are studied non-perturbatively. In particular, the Si–Si–H bending mode, for which relaxation times in the order of picoseconds have been predicted theoretically, is considered. Also, the excitation by infrared laser pulses is explicitly modelled. To do so, a combined system–bath Schrödinger equation is considered, in which an anharmonic system describing the vibrating H atom is coupled non-linearly to a set of harmonic oscillators which represent the phonon bath of the solid. For the time evolution, the multiconfigurational time-dependent Hartree (MCTDH) method is used together with a stochastic approach to sample thermal initial conditions. In contrast to perturbative approaches (Golden Rule), it is found that the bending mode relaxes the slower, the hotter the surface is. Possible reasons for this "puzzle", which also seems at variance with measurements for H:Si(100), are discussed.

Keywords MCTDH · Multiconfigurational time-dependent Hartree method · Hydrogen adsorbed on Si(100) · Random phase thermal wave function method · Temperature effects · System–bath model

Dedicated to the memory of Professor Jürgen Hinze and published as part of the Hinze Memorial Issue.

F. Lüder · P. Saalfrank (✉)
Institut für Chemie, Universität Potsdam,
Karl-Liebknecht-Straße 24-25,
14476 Potsdam-Golm, Germany
e-mail: petsaal@uni-potsdam.de

M. Nest
Theoretische Chemie, Technische Universität München,
Lichtenbergstraße 4, 85747 Garching, Germany

1 Introduction

Dynamical problems, in which a quantum "system" interacts with an environment or "bath", are ubiquitous in chemistry and physics [1, 2]. For example, in surface science the "system" can be a set of modes describing the motion of an adsorbed atom or molecule on a surface, and the "bath" consists of other adsorbate modes and surface degrees of freedom [3]. In particular, the vibrational relaxation of adsorbates due to their mechanical coupling to phonons of a surface can be described in this way.

As an example, the vibrational relaxation of the Si–H stretching and Si–Si–H bending modes of H atoms adsorbed on Si(100) surfaces has been studied in some detail by quantum dynamical modelling [4–7]. In Ref. [4] a system–bath Hamiltonian based on force fields was constructed, in which a two-mode "system" (the Si–H stretching and Si–Si–H bending modes) was coupled non-linearly to single- and two-"phonon" modes of the substrate. On the experimental side, it is known that the H–Si stretching mode of H:Si(100) decays on a nanosecond timescale, the precise lifetime depending on surface temperature and on the history of sample preparation [8]. For the bending mode, no lifetime measurements are known. Theory confirms the nanosecond lifetime of the stretching, and predicts a picosecond lifetime of the bending mode [4, 5]. Also, the mode-selective vibrational excitation with infrared (IR) laser pulses prior to relaxation was modelled theoretically for H:Si(100) [6, 7]. Experimentally, mode- and

isotope-selective IR-pulse excitation has been demonstrated recently for the related H/D:Si(111) system [9, 10].

Traditionally, system–bath models are used in the context of *reduced* dynamics in which the bath modes are traced out and only implicitly included. One then treats only the reduced system explicitly. Energy is generally not conserved in the open system due to the coupling to the bath. Examples of reduced approaches are open-system density matrix theory, and time-dependent perturbation theory using the Golden Rule. For H:Si(100), these approaches were followed in Refs. [4, 6].

More recently, it became also possible to solve the time-dependent system–bath Schrödinger equation *directly*, by propagating multidimensional wavefunctions, comprising the combined system and bath modes, forward in time. This approach is energy conserving, and free of assumptions usually made in reduced models, notably the neglect of memory effects in the Markov approximation [1, 2]. The direct solution of system–bath problems can be done efficiently (at least if the number of environmental modes is not too large), by the multiconfigurational time-dependent Hartree (MCTDH) method [11, 12]. This method was applied in Ref. [5] for the problem of vibration–phonon coupling in H:Si(100), with the two-mode system model coupled to up to 50 bath oscillators. An even larger number of bath modes can be included by using the time-dependent self-consistent field (TDSCF) method which is a single-configuration variant of MCTDH. In Ref. [6], the IR vibrational excitation of H:Si(100) has been studied with TDSCF by coupling the 2D system to more than 500 surface oscillators.

Still, direct methods to solve coupled system–bath Schrödinger equations are costly. The MCTDH method, for example, scales exponentially with the number of degrees of freedom. Also, in contrast to reduced models the inclusion of finite temperature is non-trivial, because in coherent wavepacket methods such as MCTDH one has to incoherently average over all thermally occupied initial states. If n quantum states are populated in average and if F modes are considered, one needs to propagate n^F wavepackets and average in a "brute force" approach. This is of course impossible for realistic problems. This bottleneck can be overcome by stochastic sampling schemes, such as the *random phase thermal wave function* (RPTWF) method [13]. Here, only stochastically selected wavepackets are considered and multi-dimensional problems at finite temperature can be converged with much less effort. The method has also been used in conjunction with MCTDH, for atom scattering from thermal surfaces [14].

In this paper we extend our previous investigation of vibrational relaxation in H:Si(100) using MCTDH [5], which was carried out at $T = 0$ K, to finite temperature, by adopting the MCTDH–RPTWF method. Further, we explicitly include the vibrational *excitation* by IR laser pulses in the MCTDH dynamics, while in Ref. [5] only a sudden, initial excitation had been assumed. The paper is organized as follows. In Sect. 2 the main ingredients of our model for vibration–phonon coupling in H:Si(100) will be reiterated. Computational details of MCTDH and the RPTWF approach will be given in Sect. 3. In Sect. 4 results will be presented, for the relaxation of the Si–Si–H bending mode at finite temperatures, with and without explicit inclusion of IR laser pulse excitation. Section 5 concludes and summarizes this work.

2 Model

The model used to evaluate the vibration–phonon coupling is presented in detail in Ref. [4]. The total Hamiltonian $\hat{H}$ of the H:Si(100) surface is written in the system–bath form

$$\hat{H} = \hat{H}_{\mathrm{s}} + \hat{H}_{\mathrm{b}} + \hat{H}_{\mathrm{sb}}, \tag{1}$$

where $\hat{H}_{\mathrm{s}}$ is the (sub-)system Hamiltonian, $\hat{H}_{\mathrm{b}}$ is the bath Hamiltonian, and $\hat{H}_{\mathrm{sb}}$ the system–bath coupling. The vibrational motion of a hydrogen atom on a Si dimer of the H:Si(100)(2 × 1) surface is represented by two "system" coordinates, the H–Si stretching mode r, and the bending angle ϕ of the H–Si bond with respect to the Si surface dimer, as shown in Fig. 1a. (The second bending mode is not included in the system and behaves similar to the first one.) The system Hamiltonian used here is

$$\hat{H}_{\mathrm{s}} = -\frac{\hbar^2}{2m}\frac{\partial^2}{\partial r^2} - \frac{\hbar^2}{2mr^2}\frac{\partial^2}{\partial \phi^2} + V(r,\phi). \tag{2}$$

Here $m = 1{,}836$ a.m.u. is the mass of the hydrogen atom, and $V(r, \phi)$ a two-dimensional model potential chosen as

$$V(r,\phi) = D\left(\mathrm{e}^{-2\alpha(r-r_0)} - 2\mathrm{e}^{-\alpha(r-r_0)}\right) + D + \frac{k}{2}\mathrm{e}^{-\beta(r-r_0)^2}(\phi-\phi_0)^2. \tag{3}$$

The parameters of the potential are, for completeness, summarized in the caption to Fig. 1. Here it suffices to say that r_0 and ϕ_0 are the equilibrium distances and angles of adsorbed hydrogen.

Vibrational eigenstates of the system Hamiltonian (Eq. 2) are obtained by diagonalization with the sinc-function discrete-variable-representation (DVR) method [16]. The lowest of these eigenstates can be classified as $\psi_{(n_r,n_\phi)}(r,\phi)$ by quantum numbers of the stretching mode (n_r) and bending mode (n_ϕ), respectively. The fundamental vibrational frequencies (in wavenumbers) of the bending and stretching modes are $\omega_\phi = (\varepsilon_{(0,1)} - \varepsilon_{(0,0)})/\hbar = 637\,\mathrm{cm}^{-1}$, and $\omega_r = (\varepsilon_{(1,0)} - \varepsilon_{(0,0)})/\hbar = 2{,}037\,\mathrm{cm}^{-1}$. This is in reasonable agreement with the experimental values of 630 and 2,100 cm^{-1}, respectively [8].

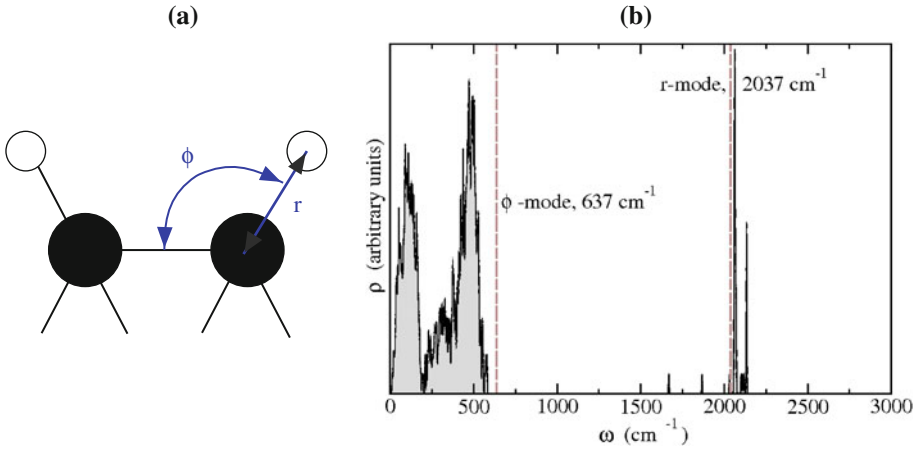

Fig. 1 **a** Schematic representation of a fragment of the H-covered Si(100) surface showing a Si dimer and the system coordinates r and ϕ (H *white*, Si *black*). The system potential is given by Eq. 3, with parameters $D = 0.25\ \mathrm{E}_h$ (well depth, $1\ \mathrm{E}_h = 1$ Hartree = 27.211 eV), $\alpha = 0.83\ \mathrm{a}_0^{-1}$ ($1\ \mathrm{a}_0 = 1$ Bohr = 0.52918 Å), $r_0 = 2.84\ \mathrm{a}_0$ (equilibrium Si–H bond length), $k = 3.90 \times 10^{-5}\ \mathrm{E}_h/\mathrm{deg.}^2$ (force constant), $\phi_0 = 112.6°$ (equilibrium Si–Si–H bond angle), $\beta = 0.2\ \mathrm{a}_0^{-2}$. **b** Density of states of vibrational bath modes, obtained from a normal mode analysis of a cluster $Si_{144}H_{36}$ modelling H:Si(100) as described in the text. *Vertical dashed lines* define the fundamental frequencies of the stretching (r) and bending modes (ϕ)

The bath consists of harmonic oscillators with frequencies ω_i and masses M_i which are obtained from the normal mode analysis (NMA) of a cluster model representing a fully H-covered Si substrate. Specifically, a $Si_{144}H_{36}$ cluster in a slab geometry (i.e. with $N_{at} = 180$ atoms in total) was used; see Fig. 1c of Ref. [4]. To obtain the normal modes, the semi-empirical bond order potential by Dyson and Smith was adopted [17, 18]. When broadened by Lorentzians of width 1 cm^{-1}, one obtains the density of states ρ of the "phonon bath" as shown in Fig. 1b. Also indicated in the figure, as dashed lines, are the fundamental frequencies ω_r and ω_ϕ of the isolated system. These frequencies lie outside the main "phonon" band of the Si(100) substrate, with a Debye frequency of 580 cm^{-1} [5]. The bath Hamiltonian thus reads

$$\hat{H}_\mathrm{b} = \sum_i^{N_B} \left(-\frac{\hbar^2}{2M_i} \frac{\partial^2}{\partial q_i^2} + \frac{1}{2} M_i \omega_i^2 q_i^2 \right), \tag{4}$$

where q_i are the normal mode coordinates, which are linear combinations of Cartesian displacements of each cluster atom, and $N_B = 3N_{at} - 6 = 534$ is the number of the bath oscillators. For the MCTDH calculations below, only a subset of N of these surface oscillators was included (see Sect. 3.1).

The system–bath coupling Hamiltonian is given as

$$\hat{H}_\mathrm{sb} = \sum_i^{N_B} \lambda_i(r,\phi) q_i + \frac{1}{2} \sum_i^{N_B} \sum_j^{N_B} \Lambda_{ij}(r,\phi) q_i q_j \tag{5}$$

and contains two parts. The first part, involving a single sum, accounts for adsorbate relaxation involving excitation of a single substrate phonon. The single-phonon coupling functions $\lambda_i(r, \phi)$ depend on system coordinates, and were obtained by Taylor expansion of the semi-empirical force field. The second, double sum describes relaxation processes involving two substrate phonons, with the two-phonon coupling functions $\Lambda_{ij}(r, \phi)$. All couplings are non-linear in the system modes, but (bi-)linear in substrate phonon modes. Since the fundamental system frequencies ω_r and ω_ϕ lie outside the phonon band of the bath (see above), the single-phonon terms alone cannot account for vibrational relaxation of the system vibrational states. In fact, they play only a minor role compared to the two-phonon terms and can, at least for low-energy excitations to be studied below, be safely neglected. In passing, we note that the bath modes are only indirectly coupled to each other through their coupling to the system modes.

To account for IR laser excitation of the system modes, the system Hamiltonian $\hat{H}_\mathrm{s}$ in Eq. 2 is extended as

$$\hat{H}_\mathrm{s} \rightarrow \hat{H}_\mathrm{s} - \mu_z(r,\phi) E_z(t). \tag{6}$$

We assume a laser polarized perpendicular to the surface (in z-direction). $E_z(t)$ is the laser field, for which so-called π-pulses for the excitation of the bending mode will be used. $E_z(t)$ is chosen to have a $\sin^2$ temporal shape:

$$E_z(t) = E_0 \sin^2\left(\frac{\pi t}{t_p}\right) \sin(\omega_\phi t). \tag{7}$$

Here, t_p is the total pulse duration and ω_ϕ the laser carrier frequency which is resonant with the fundamental ϕ-transition. E_0 is the amplitude of the pulse, for a π-pulse of the form (Eq. 7) given as $2\pi\hbar/t_p\mu_{if}$. Here, μ_{if} is the transition dipole moment connecting initial and target state, i.e. $\mu_{if} = \langle\phi_{(0,0)}|\mu_z|\phi_{(0,1)}\rangle$ below. The z-component of the dipole function, $\mu_z(r, \phi)$, was chosen as

$$\mu_z(r,\phi) = A_0 + A_1(r-r_0)\mathrm{e}^{-A_2(r-r_0)} + A_3(\phi-\phi_0) \qquad (8)$$

with parameters $A_0 = 0.4001$ ea$_0$, $A_1 = -1.2587$ e, $A_2 = 0.3175$ a$_0^{-1}$, $A_3 = -0.4734$ ea$_0$/rad (1 rad = 360°/2π), and the equilibrium values r_0 and ϕ_0 as defined above. The parametrization (Eq. 8) results from cluster calculations and density functional theory as outlined elsewhere [6]. No direct coupling of the laser pulse to the bath oscillators is assumed.

3 Simulation details

3.1 MCTDH calculations

The solution of the system–bath Schrödinger equation

$$i\hbar\frac{\partial\Psi}{\partial t} = \left(\hat{H}_\mathrm{s} + \hat{H}_\mathrm{b} + \hat{H}_\mathrm{sb}\right)\Psi \qquad (9)$$

was carried out with the help of the Heidelberg MCTDH program package [12]. For our specific system–bath problem with two system degrees of freedom and N bath oscillators, the MCTDH wavefunction is

$$\Psi(r,\phi,q_1,\ldots,q_N,t) = \sum_{j_r=1}^{n_r}\sum_{j_\phi=1}^{n_\phi}\sum_{j_1=1}^{n_1}\cdots\sum_{j_N=1}^{n_N} A_{j_r j_\phi j_1,\ldots j_N}(t) \times \varphi_{j_r}^{(r)}(r,t)\varphi_{j_\phi}^{(\phi)}(\phi,t)\prod_{\kappa=1}^{N}\varphi_{j_\kappa}^{(\kappa)}(q_\kappa,t). \qquad (10)$$

Here, the A's are time-dependent expansion coefficients, and the $\varphi_{j_\kappa}^{(\kappa)}$ coordinate- and time-dependent single-particle functions (SPFs) for the κth degree of freedom. There are n_κ SPFs for mode κ. The Dirac–Frenkel variational principle leads to equations of motion for the coefficients and single-particle functions, as detailed elsewhere [11, 12].

To allow for systematic studies, the number of bath oscillators N was restricted to $N = 20$. These oscillators were selected according to an energy conservation argument in combination with a coupling-strength criterion. Accordingly, only those pairs of bath oscillators are considered whose energies obey the relation

$$|\varepsilon_m - \varepsilon_n| - \gamma \le \hbar|\omega_i + \omega_j| \le |\varepsilon_m - \varepsilon_n| + \gamma, \qquad (11)$$

where ω_i and ω_j are the frequencies of the bath modes i and j, ε_m and ε_n are the subsystem energy levels of interest ($\varepsilon_m - \varepsilon_n = \hbar\omega_\phi$ in our case), and $\gamma = 8$ cm^{-1} is a parameter, related to the width of the approximated δ-function in a perturbative treatment of the relaxation process [5]. The pairs of oscillators (i,j) are then sorted in the decreasing order of their coupling strength to the system modes, as outlined in Ref. [5]. In the following, the 20 oscillators with frequencies ω_i and masses M_i as shown in Table 1 are used. Therefore, the system–bath Schrödinger equation (Eq. 9) is 22-dimensional.

Table 1 Frequencies and masses of the 20 bath oscillators used in this work

Mode	ω (cm^{-1})	M (a.m.u.)	Mode	ω (cm^{-1})	M (a.m.u.)
q_1	122.449	36,880.2	q_{11}	411.732	4,289.3
q_2	129.480	37,941.3	q_{12}	412.513	4,892.4
q_3	134.528	39,873.0	q_{13}	413.149	7,635.2
q_4	142.342	28,283.4	q_{14}	419.760	7,058.2
q_5	164.969	33,965.4	q_{15}	464.724	4,257.7
q_6	165.296	36,290.1	q_{16}	468.271	4,679.6
q_7	167.644	32,237.4	q_{17}	470.614	5,981.9
q_8	221.810	13,851.6	q_{18}	495.645	12,036.2
q_9	231.870	5,786.1	q_{19}	505.694	13,317.5
q_{10}	399.807	9,482.2	q_{20}	509.205	11,645.7

A further reduction of computational effort can be achieved by *mode combination* [12, 15]. Accordingly, we merge several of the bath modes into a single combined mode, S_j. In the present work, a total number of four combined modes $j = 1,\ldots,4$ was used, namely $S_1 = \{q_2; q_3; q_{10}; q_{12}; q_{19}\}$, $S_2 = \{q_1; q_4; q_6; q_{18}; q_{20}; q_{11}\}$, $S_3 = \{q_8; q_9; q_{13}; q_{14}\}$, and $S_4 = \{q_5; q_7; q_{15}; q_{16}; q_{17}\}$. The MCTDH wave function with mode combination is thus

$$\Psi(r,\phi,S_1,S_2,S_3,S_4,t) = \sum_{j_r=1}^{n_r}\sum_{j_\phi=1}^{n_\phi}\sum_{j_1=1}^{\tilde{n}_1}\ldots\sum_{j_4=1}^{\tilde{n}_4} A_{j_r j_\phi j_1,\ldots j_4}(t) \times \varphi_{j_r}^{(r)}(r,t)\varphi_{j_\phi}^{(\phi)}(\phi,t)\prod_{\kappa=1}^{4}\varphi_{j_\kappa}^{(\kappa)}(S_\kappa,t), \qquad (12)$$

where $\tilde{n}_j$ denotes the number of SPFs for combined mode j. The system modes r and ϕ and the combined modes S_j are all represented on time-independent DVR grids, with parameters and DVR-types given in Table 2. Also indicated in the table are the numbers of single-particle functions n (or $\tilde{n}$) for each (combined) mode. The total number of configurations was 298,116.

As initial states for the propagation, we take a Hartree product of one-dimensional wavefunctions of the type

$$\Psi(r,\phi,\{q_i\};t=0) = \chi_{n_r}^{(r)}(r)\chi_{n_\phi}^{(\phi)}(\phi)\prod_{i=1}^{N}\tilde{\psi}_{n_i}^{(i)}(q_i). \qquad (13)$$

Let us consider the situation for zero temperature, $T = 0$ first. Then all bath modes q_i are initially in their ground state ($n_i = 0$), and the wavefunctions $\tilde{\psi}_0^{(i)}(q_i)$ are ground state harmonic oscillator functions. The initial state of the system is a product of zero-order wavefunctions $\chi_{n_r}^{(r)}(r)$ and $\chi_{n_\phi}^{(\phi)}(\phi)$, which we will also denote as $\chi_{n_r}^{(r)}\cdot\chi_{n_\phi}^{(\phi)} = |n_r\, n_\phi\rangle$ for short. Two different initial quantum numbers for n_r and n_ϕ were chosen: when excitation by IR pulses was modelled, we start from the ground state by setting $n_r = n_\phi = 0$. If the decay of a pre-excited adsorbate (in the ϕ mode) is of interest, then the choice $n_r = 0$ and $n_\phi = 1$ was made instead. Pre-excitation

Table 2 DVR parameters for MCTDH calculation

Mode	DVR	Minimum	Maximum	N_p	n ($\tilde{n}$)
r	sin	1.7 a_0	5.7 a_0	30	3
ϕ	sin	1.1 a_0	2.8 a_0	40	3
S_1 (5 modes)	HO			5, 3, 4, 4, 4	13
S_2 (6 modes)	HO			5, 3, 3, 3, 3, 7	13
S_3 (4 modes)	HO			6, 6, 4, 4	14
S_4 (5 modes)	HO			4, 4, 4, 4, 4	14

The choice of the DVR is presented, with sin being the sinc-function-DVR [16] and HO standing for Gauß-Hermite-DVR. Minimum and maximum define grid extensions for the system modes, N_p is the number of grid points. The number of SPFs for a given mode is denoted as n (for r and ϕ), or $\tilde{n}$ (for the combined bath modes)

of the r-mode was not considered, because this mode relaxes too slowly to be efficiently handled by MCTDH [5]. The zero-order states in Eq. 13 are calculated from one-dimensional Schrödinger equations

$$\left[-\frac{\hbar^2}{2m}\frac{\mathrm{d}^2}{\mathrm{d}r^2}+V(r,\phi_0)\right]\chi_{n_r}^{(r)}(r)=\epsilon_{n_r}\chi_{n_r}^{(r)}(r) \tag{14}$$

$$\left[-\frac{\hbar^2}{2mr_0^2}\frac{\mathrm{d}^2}{\mathrm{d}\phi^2}+V(r_0,\phi)\right]\chi_{n_\phi}^{(\phi)}(\phi)=\epsilon_{n_\phi}\chi_{n_\phi}^{(\phi)}(\phi). \tag{15}$$

Note that the product of zero-order states $\chi_{n_r}^{(r)}(r)\cdot\chi_{n_\phi}^{(\phi)}(\phi)$ in Eq. 13 is not an exact 2D eigenfunction ϕ of the system Hamiltonian, but close to it, i.e. $\chi_{n_r}^{(r)}(r)\cdot\chi_{n_\phi}^{(\phi)}(\phi)\approx\psi_{(n_r,n_\phi)}(r,\phi)$, and $\varepsilon_{(n_r,n_\phi)}\approx\varepsilon_{n_r}+\varepsilon_{n_\phi}$. Using exact system-eigenstates, e.g. $\psi_{(0,0)}$ or $\psi_{(0,1)}$ instead, is not expected to influence the results significantly [6]. Finite temperatures will be treated by the MCTDH–RPTWF method as described in Sect. 3.2.

Among the observable quantities of interest in this study are the expectation values of the system, bath and interaction energy $\langle\hat{H}_\mathrm{s}\rangle$, $\langle\hat{H}_\mathrm{b}\rangle$ and $\langle\hat{H}_\mathrm{sb}\rangle$, respectively. These are easily evaluated with the Heidelberg MCTDH package as outlined elsewhere [15]. Here, we only note that the definition of $\langle\hat{H}_\mathrm{sb}\rangle$ is not strictly unique.

The analysis of the populations of subsystem energy levels is done as follows. We first extract one-dimensional subsystem density operators $\hat{\rho}_r(r,r';t)$ and $\hat{\rho}_\phi(\phi,\phi';t)$ in coordinate representation, out of the time-dependent wavefunctions $|\Psi(t)\rangle$ in MCTDH form:

$$\hat{\rho}_r(r,r';t)=\mathrm{Tr}_{B,\phi}\{|\Psi(t)\rangle\langle\Psi(t)|\} \tag{16}$$

$$\hat{\rho}_\phi(\phi,\phi';t)=\mathrm{Tr}_{B,r}\{|\Psi(t)\rangle\langle\Psi(t)|\} \tag{17}$$

(with B denoting the bath modes). We then project on the one-dimensional zero-order states $|\chi_{n_r}^{(r)}\rangle$ or $|\chi_{n_\phi}^{(\phi)}\rangle$, i.e.

$$P_{n_r}=\mathrm{Tr}_r\left\{\hat{\rho}_r^\dagger(t)|\chi_{n_r}^{(r)}\rangle\langle\chi_{n_r}^{(r)}|\right\} \tag{18}$$

$$P_{n_\phi}=\mathrm{Tr}_\phi\left\{\hat{\rho}_\phi^\dagger(t)|\chi_{n_\phi}^{(\phi)}\rangle\langle\chi_{n_\phi}^{(\phi)}|\right\}. \tag{19}$$

We thus obtain the populations of states with quantum numbers n_r or n_ϕ, irrespective of all other quantum numbers. In many cases below, the r-mode remains unexcited, then P_{n_ϕ} is equivalent to the population of the 2D system state $|0,n_\phi\rangle$, i.e. $P_{n_\phi}=P_{(0,n_\phi)}$. Using zero-order states for analysis rather than exact two-dimensional subsystem wavefunctions introduces a small error, but allows for a rigorous definition of vibrational quantum numbers.

Using the one-dimensional subsystem density operators $\hat{\rho}_r$ and $\hat{\rho}_\phi$, we can also define mode-resolved system energies $\langle\hat{H}_r\rangle$ and $\langle\hat{H}_\phi\rangle$ as

$$\langle\hat{H}_r\rangle=\mathrm{Tr}_r\{\hat{\rho}_r^\dagger(t)\hat{H}_r\} \tag{20}$$

$$\langle\hat{H}_\phi\rangle=\mathrm{Tr}_\phi\left\{\hat{\rho}_\phi^\dagger(t)\hat{H}_\phi\right\}. \tag{21}$$

Since the system modes are not separable, we define

$$\hat{H}_\phi=-\frac{\hbar^2}{2mr_0^2}\frac{\mathrm{d}^2}{\mathrm{d}\phi^2}+\frac{k}{2}\mathrm{e}^{-\beta(r-r_0)}(\phi-\phi_0)^2 \tag{22}$$

$$\hat{H}_r=-\frac{\hbar^2}{2m}\frac{\mathrm{d}^2}{\mathrm{d}r^2}+D(\mathrm{e}^{-2\alpha(r-r_0)}-2\mathrm{e}^{-\alpha(r-r_0)})+D, \tag{23}$$

i.e. the potential coupling between r and ϕ is counted for the ϕ-mode. Still, the relation $\hat{H}_\mathrm{s}=\hat{H}_r+\hat{H}_\phi$ does not hold exactly, therefore $\langle\hat{H}\mathrm{s}\rangle=\langle\hat{H}_r\rangle+\langle\hat{H}_\phi\rangle$ does not hold exactly either, but to a good approximation (see below).

3.2 The MCTDH–RPTWF method

In the *random phase thermal wave function* method, we wish to describe a thermal ensemble described by the density operator

$$\hat{\rho}(\beta)=\frac{\mathrm{e}^{-\beta\hat{\mathrm{H}}}}{Z}, \tag{24}$$

where $\beta=\frac{1}{k_BT}$, Z is the partition function $Z=Tr\{\mathrm{e}^{-\beta\hat{H}}\}$. In the RPTWF method one first creates a wavefunction Φ corresponding to the limit of infinite temperature. The wavefunction Φ is expanded as

$$|\Phi(\vec{\theta})\rangle=\frac{1}{\sqrt{L}}\sum_l^L\mathrm{e}^{i\theta_l}|\phi_l\rangle, \tag{25}$$

where $\{\phi_l\}$ is a complete basis. Further, $\mathrm{e}^{i\theta_l}$ are random phase factors with random numbers θ_l in the interval $[0,2\pi]$, L is the number of basis functions, and $\vec{\theta}$ a vector of length L which contains all θ_l. The unity operator can be written as a sum over projectors on the random phase wavefunctions,

$$\hat{I}=\lim_{K\to\infty}\frac{1}{K}\sum_{k=1}^K|\Phi(\vec{\theta}_k)\rangle\langle\Phi(\vec{\theta}_k)|, \tag{26}$$

where k labels different stochastic realizations. Inserting this into the definition of Eq. 24 one gets

$$\hat{\rho}(\beta) = \frac{1}{Z} e^{-(\beta/2)\hat{H}_0} \hat{I} e^{-(\beta/2)\hat{H}_0} = \lim_{K\to\infty} \frac{1}{Z}\frac{1}{K}\sum_{k=1}^{K} |\Phi(\beta/2, \vec{\theta}_k)\rangle\langle\Phi(\beta/2, \vec{\theta}_k)|. \quad (27)$$

$\hat{H}_0$ is usually the full Hamiltonian, but specific exceptions will be introduced below. In Eq. 27, the random phase thermal wave function $|\Phi(\beta/2, \vec{\theta}_k)\rangle$ is obtained by propagating the wavefunction $|\Phi(\vec{\theta})\rangle$ of Eq. 25 in imaginary time up to $\beta/2$, which corresponds to "cooling" the system to the required temperature. Expectation values of observables, described by operators $\hat{A}$, can then be calculated as

$$\langle\hat{A}\rangle = Tr\{\hat{\rho}^{\dagger}\hat{A}\} = \lim_{K\to\infty} \frac{1}{Z}\frac{1}{K}\sum_{k=1}^{K}\langle\Phi(\beta/2, \vec{\theta}_k)|\hat{A}|\Phi(\beta/2, \vec{\theta}_k)\rangle. \quad (28)$$

Specifically, for the implementation of this scheme in MCTDH the following four steps are necessary [13]:

1. A wave function with random phase at infinite temperature is constructed. For this purpose, the coefficients for each configuration of the MCTDH wave function $A_{j_1,\ldots,j_F}$ are chosen as complex numbers $e^{i\theta_l}$, with random phases $\theta_l, \in [0, 2\pi]$.
2. This wave function is propagated in imaginary time to $\beta/2$. Now the eigenstates of the system are populated according to a Boltzmann distribution (in the limit of an infinite number of SPFs).
3. The wave function constructed in this way is propagated in real time.
4. The steps 1 to 3 are repeated, until the expectation values of interest are converged.

Since in practice we work with a finite basis set here, the definition of "temperature" is associated with some error, which has been quantified, for a different problem, in Ref. [13].

4 Results and discussion

4.1 Simulations at zero temperature

4.1.1 Excited system eigenstates as initial states

To set the stage, we start with simulations for $T = 0$ K, and study the vibrational relaxation of a state which was pre-excited (with one quantum) in the bending mode. Thus, the system part of the initial wavefunction Eq. 13 is given as

$$\chi_{n_r}^{(r)} \cdot \chi_{n_\phi}^{(\phi)} = |0, 1\rangle, \quad (29)$$

and for the bath oscillators we have $\{n_i\} = 0$. Due to the coupling to the bath modes, the system state $|0, 1\rangle$ is non-stationary and "decays". This is indicated in Fig. 2, where results of a single MCTDH propagation up to 4 ps (4,000 fs) are shown for populations $P_{n\phi} = 1$ (a), and system energies $\hat{H}_s$ (b).

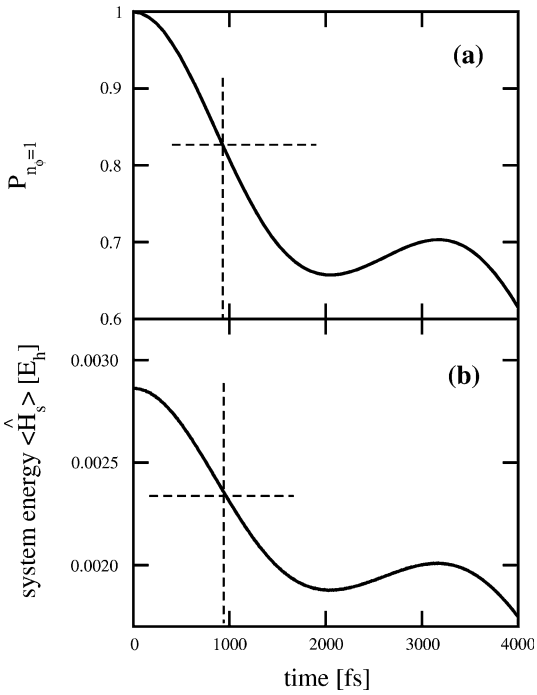

Fig. 2 **a** The population $P_{n_\phi=1}$ as defined in Eq. 19, for the initial system state $|0, 1\rangle$ used in Eq. 13. **b** Corresponding expectation value of the system energy, $\hat{H}_s$. The vertical dashed lines denote the definition of a time $\tilde{\tau}$ as a measure for the "lifetime", as explained in the text

From Fig. 2b we see that energy of the subsystem is transferred to the bath. (The excitation of the *r*-mode is found to be negligible [5].) The energy scale in the figure is relative to the energy of the zero-order ground states, i.e. state (Eq. 13) with the choice $n_r = n_\phi = n_i = 0$. The ϕ-mode has a fundamental frequency of 637 cm^{-1}, or 2.9×10^{-3} E_h which is the initial energy of the ϕ-excited system. From the figure, the following information can be drawn:

(1) The decay is non-exponential. In particular, the slope $d\langle\hat{H}_s\rangle/dt$ is zero in the limit $t \to 0$ and not finite as expected for an exponential energy loss.

(2) $\langle\hat{H}_s\rangle$ decays monotonically up to about $t = 2$ ps, and then rises due to a *recurrence*. Recurrences are characteristic for a *finite bath*. For an ideal bath with equidistant frequency spacing $\Delta\omega$ one expects a recurrence time of $T_{rec} = 2\pi/\Delta\omega$ [19]. For 20 surface oscillators in an energy range up to about 500 cm^{-1} (see Table 1), we estimate an average $\Delta\omega \approx 500/20 = 25$ cm^{-1}. This gives $T_{rec} \approx 1.3$ ps and therefore the right order of magnitude. In Ref. [5] the

dependence of the recurrence time on the number of bath oscillators was systematically investigated. It was found that with ≥40 surface oscillators, the decay of $|0, 1\rangle$ is still monotonic up to 4 ps (albeit already decelerated above ∼2 ps).

(3) For our 20-oscillator bath we also note that up to $t \approx 2$ ps, only about 1/3 of the initial excitation energy of 2.9×10^{-3} E_h is actually transferred to the bath, because the latter is non-resonant with the energy difference between the initial and final system state.

Due to (1)–(3), an exact vibrational lifetime τ of state $|0, 1\rangle$ cannot be defined. As a simple measure for the decay time, we take the time $\tilde{\tau}$ after which half of an energy loss ΔE has occurred instead. Here, ΔE is the difference between the system energy at $t = 0$, and the system energy at the first (recurrence) minimum. In the example of Fig. 2b, we find $\tilde{\tau} = 0.96$ ps; see the dashed, vertical line in the figure. This approximate definition of a relaxation time will in general depend on the size of the bath.

From Fig. 2a where $P_{n_\phi=1}(t)$ is shown, we note that the energy loss is accompanied by a corresponding loss of population for states with $n_\phi = 1$. Since the r-mode remains unexcited, the figure reflects the relaxation from system state $|0, 1\rangle$ to state $|0, 0\rangle$. Also, here a recurrence occurs, and the "lifetime" defined similarly as above yields the same value as the energy criterion, $\tilde{\tau} = 0.96$ ps.

All of this is in agreement with Ref. [5], where, using similar models, vibrational "lifetimes" in the order of picoseconds have been predicted for the bending mode of H:Si(100). In Ref. [5] it was also seen that the lifetimes of excited initial system states $|0, n_\phi\rangle$, scale approximately as $\tilde{\tau}(n_\phi) \approx \tilde{\tau}(n_\phi = 1)/n_\phi$. This scaling is expected from perturbation theory in the linear-coupling limit [4]. In Ref. [5] it was further demonstrated that r-excited initial states, e.g. $|1, 0\rangle$, do not significantly decay on a picosecond timescale. This is in agreement with the nanasecond lifetime of the Si–H stretch as observed/predicted elsewhere [4, 8]. The three orders of magnitude difference for the bending and stretching lifetimes have been interpreted in Ref. [4] as being due to the fact that the high-frequency stretching mode relaxes initially by exciting the bending mode to which it is only weakly coupled. In contrast, the bending mode relaxes directly by coupling to surface phonon modes, which is a faster process.

4.1.2 *Infrared excitation from the ground state*

To account for the simultaneous infrared excitation in a real experiment, $\sin^2$-shaped π-pulses in resonance with the ϕ-mode as indicated in Eq. 7 were used. We start from the ground state at $T = 0$ K, well represented by the zero-order states in Eq. 13 with the choice

$$\chi_{n_r}^{(r)} \cdot \chi_{n_\phi}^{(\phi)} = |0, 0\rangle, \tag{30}$$

and $n_i = 0$ for the bath oscillators.

The π-pulse started at $t = 0$, with a total duration of $t_p = 1$ ps. With the computed value of the transition dipole moment for the $|0, 0\rangle \rightarrow |0, 1\rangle$ excitation of 5.06×10^{-2} ea_0 [6], the π-pulse field amplitude is $E_0 = 3.00 \times 10^{-3}$ E_h/ea_0, corresponding to a peak intensity of $I_{max} = 2.05 \times 10^{10}$ W/cm^2. π-pulses are known to induce a complete population inversion in a dissipation-free two-level system [6].

From Fig. 3a we learn that this is not the case for the problem at hand. In the figure, the populations of various ϕ-excited states are shown, as a function of time. We recognize that the $|0, 0\rangle$ state is depopulated on the time-scale of the pulse of 1 ps, as expected. However, the depopulation after the pulse end is incomplete, with about

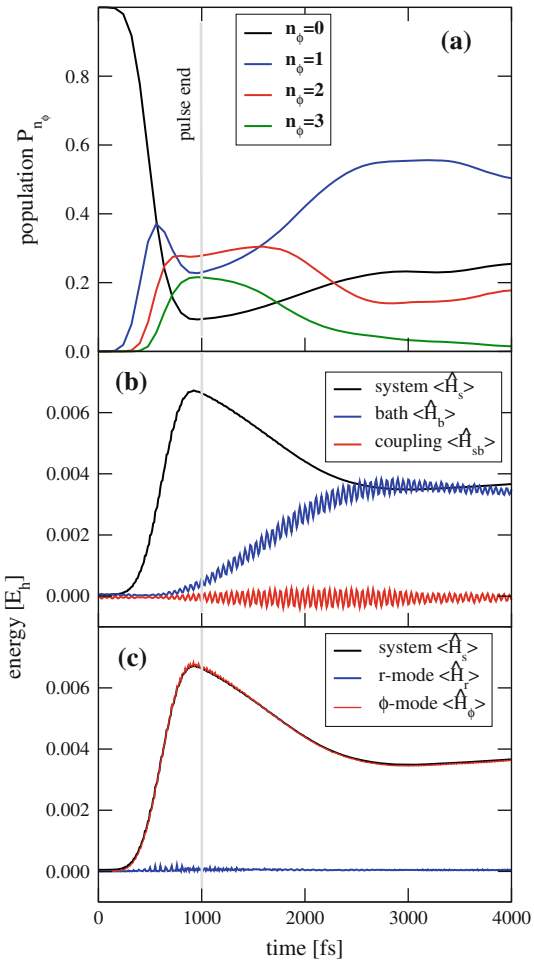

Fig. 3 **a** Population $P_{n_\phi}(= P_{(0,n_\phi)})$ for various selected states, when a 1 ps π-pulse resonant with the ϕ-mode is applied (see text). Corresponding energy expectation values $\langle \hat{H}_s \rangle$, $\langle \hat{H}_b \rangle$ and $\langle \hat{H}_{sb} \rangle$ **b** and $\langle \hat{H}_\phi \rangle$ and $\langle \hat{H}_r \rangle$ **c** as defined in the text. The *vertical grey line* gives the end of the laser pulse

10% of population left in the initial state. Also higher excited ϕ-states such as $|0, 2\rangle$ and $|0, 3\rangle$ are populated during the pulse, to a non-negligible extent. The r-mode remains unexcited also in this example (see below), which is why the assignment $n_r = 0$ for the r-quantum number is valid. As a result, after $t = t_p = 1$ ps the first three excited ϕ-states are about equally populated. Thus, the excitation is not state-selective, which is due to the fact that the model potential $V(r, \phi)$ (Eq. 3) is very harmonic in the ϕ-mode. A similar behaviour was found in earlier reduced-density matrix models for the same system [6].

Despite being non-state selective, the pulse is *mode-selective*: Only the system, and here in particular only the ϕ-mode is excited. This can be seen from Fig. 3b, where we show changes in energy expectation values $\langle \hat{H}_s \rangle$, $\langle \hat{H}_b \rangle$ and $\langle \hat{H}_{sb} \rangle$, and from Fig. 3c, where the state-resolved system energies $\langle \hat{H}_\phi \rangle$ and $\langle \hat{H}_r \rangle$ are given. From Fig. 3b we recognize that indeed during the pulse almost only the system modes are excited, while the bath remains "cold". Figure 3c shows that in particular the ϕ-mode is excited, as desired, while the r-mode remains unaffected. Thus, the IR pulse is mode-selective as stated above. Note that the system energy gain of 0.0066 E_h at $t \approx t_p$ exceeds the energy of $\hbar\omega_\phi$ =0.0029 E_h, due to the excitation of overtones.

After the pulse is off, "energy relaxation" by vibration–phonon coupling sets in. This is most clearly seen in Fig. 3b, where for times $t > t_p$ the system energy is found to drop to lower values. Again, a recurrence is seen at a longer time. More precisely, the maximum energy is 6.57×10^{-3} E_h at $t = 920$ fs, and the first minimum is 3.39×10^{-3} E_h at $t = 3{,}010$ fs. One can define a "lifetime", $\tilde{\tau}$, along similar lines as in Sect. 4.1.1, with the time-zero taken as $t = 920$ fs, where $\langle \hat{H}_s \rangle$ is maximal. In this way we obtain $\tilde{\tau} = 0.83$ ps. The slightly shorter "lifetime" as compared to $\tilde{\tau}(n_\phi = 1) = 0.96$ ps may be interpreted as arising from the fact that now several excited ϕ-states contribute to the decay, with the higher excited states decaying faster than the $n_\phi = 1$ state [5]. On the other hand, given the simplicity of the lifetime estimate it is only fair to say that also here, the energy relaxation proceeds on a picosecond timescale.

4.2 Effects of finite temperature

4.2.1 Excited system eigenstates as initial states

To investigate temperature effects, the *Random Phase Thermal Wave Function* method was used. In a first step the somewhat artificial situation is studied where initially the system is in the ϕ-excited state $|0, 1\rangle$ as in Eq. 29, while the "bath" has a certain finite temperature, T. To realize this perturbed equilibrium situation by MCTDH–RPTWF, the protocol of Sect. 3.2 is modified as follows:

1. The expansion coefficients $A_{j_r j_\phi j_{s_1} j_{s_2} j_{s_3} j_{s_4}}$ of the MCTDH wavefunction (Eq. 12) are chosen as random phases $e^{i\theta_l}$ only if $j_r = 1$ and $j_\phi = 1$. Otherwise, they are chosen as zero. In this way one creates wavefunctions in which the system modes are described by single SPFs representing state $|0, 1\rangle$, while the bath is in the $T \to \infty$ limit.
2. The random wavefunction is then propagated under the influence of a Hamiltonian $\hat{H}_0 = \hat{H}_b$ in imaginary time[1] to $t_{prop} = \hbar\beta/2$, according to Eq. 27. Thus, the subsystem parts of the Hamiltonian are not included in the thermalization procedure, i.e. the system remains in state $|0, 1\rangle$ during the bath equilibration. Temperatures in the range between 50 and 950 K were considered, corresponding to imaginary propagation times between 76 and 4 fs, respectively.
3. With the initial state created in this way, a real-time propagation is carried out, with a propagation time of 4 ps.
4. Steps (1)–(3) are repeated, and computed expectation values are averaged over K realizations.

The number of realizations required is surprisingly small. The convergence behaviour is demonstrated in Fig. 4, for averaged populations $P_{n_\phi=1}(K) = \frac{1}{K}\sum_{k=1}^{K} P^{(k)}_{n_\phi=1}$, when an increasing number of realizations K was used (k labels the individual realizations). In Fig. 4a, the temperature was $T = 100$ K, and in Fig. 4b $T = 350$ K is chosen. It is seen that with only $K = 5$ realizations the population dynamics does not change significantly anymore. At lower temperatures than 100 K, the convergence is even faster because less states are thermally populated. Interestingly, also at very high temperatures (>350 K and higher), the convergence is better than for the intermediate case $T = 100$ K, due to reasons which are explained in Refs. [13, 14]. $K = 5$ was applied for all cases below. In passing we note that a similar fast convergence of the MCTDH–RPTWF scheme has also been observed for atom-surface scattering in Ref. [14], where the sticking probability was found to be converged to better than 1% for $K = 20$.

In Fig. 5a populations of states with $n_\phi = 1$ (again in excellent approximation equal to the population of state $|0, 1\rangle$) are given. In Fig. 5b, we show the averaged system energy $\langle \hat{H}_s \rangle$ for bath temperatures $T \in [50, 950]$ K, monitoring the relaxation of the $|0, 1\rangle$ initial state of the system. The following observations are made:

[1] More precisely, in the actual equilibration procedure we chose $\hat{H}_0 = \hat{H}_b + \tilde{\hat{H}}_{sb}$ for imaginary time propagation, where $\tilde{\hat{H}}_{sb}$ is an approximate interaction Hamiltonian, in which the coupling constants $\Lambda_{ij}(r, \phi)$ (and $\lambda_i(r, \phi)$) are replaced by their values at the system equilibrium geometries, i.e. $\Lambda_{ij}(r_0, \phi_0)$ (and $\lambda_i(r_0, \phi_0)$). Since the coupling functions at equilibrium are close to zero, however, the Hamiltonian $\tilde{\hat{H}}_{sb}$ does effectively not couple the system with the bath.

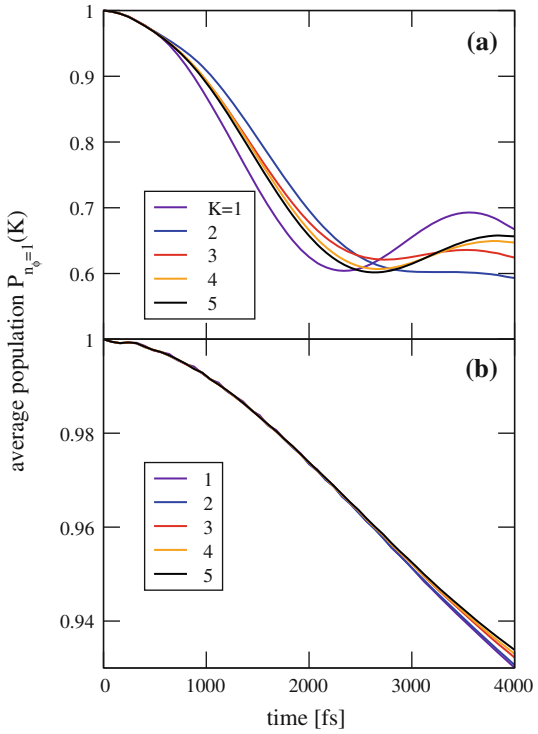

Fig. 4 Average value $P_{n_\phi=1}(K)$ as a function of time, for different numbers K of realizations of the MCTDH–RPTWF algorithm, at temperatures of $T = 100$ K (**a**), and 350 K (**b**)

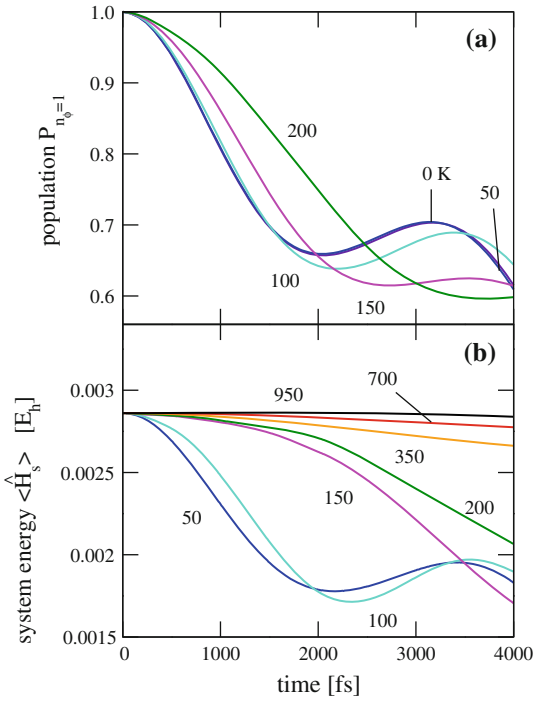

Fig. 5 **a** Averaged population $P_{n_\phi=1}$ for bath temperatures in the range 0–200 K. **b** Averaged system energy $\langle \hat{H}_s \rangle$ with the initial state $|0, 1\rangle$ and various bath temperatures in the range 50–950 K as described by the MCTDH–RPTWF algorithm. Numbers attached to the curves are temperatures in Kelvin

(1) At low temperatures, up to about $T = 100$ K, the behaviour is similar as in Fig. 2 for $T = 0$ K, i.e. one observes "relaxation" of the ϕ-mode and a recurrence on a picosecond timescale.
(2) At higher temperatures, the energy loss becomes *slower*, and the recurrences occur at later times, often beyond the propagation time of 4 ps. For the energies, already for temperatures $T > 100$ K the recurrence does not occur within the first 4 ps anymore. For the populations, recurrence times smaller than 4 ps are found up to about 200 K. Using the procedure from above, we can estimate "lifetimes" from the populations in this regime, as $\tilde{\tau}(0\,\mathrm{K}) = 0.92$ ps, $\tilde{\tau}(50\,\mathrm{K}) = 0.92$ ps, $\tilde{\tau}(100\,\mathrm{K}) = 1.00$ ps, $\tilde{\tau}(150\,\mathrm{K}) = 1.24$ ps, and $\tilde{\tau}(250\,\mathrm{K}) = 2.09$ ps. Above this temperature, the relaxation slows down even further, as it is evident from Fig. 5b.
(3) Closer inspection shows that for the highest temperature studied, $T = 950$ K, initially the system energy even *increases*. In this case the bath is so "hot" that energy is transferred into the system modes.

In general, the slower transfer of energy from system to bath modes at high T can be explained by the fact that a "hot" surface has a decreasing tendency to accept energy from the excited subsystem. We will return to this point shortly.

4.2.2 *Infrared excitation from a thermal initial state*

We now study the more realistic case, that initially bath *and* subsystem are in thermal equilibrium, and that a laser pulse is needed to excite the system. The preparation of the thermal initial state is done following the MCTDH–RPTWF protocol of Sect. 3.2. The IR laser pulse excitation is modelled by real-time propagation for 4 ps, starting from the thermalized initial state. The IR laser pulse is the same as before, i.e. a π-pulse with 1 ps duration. Temperatures up to 350 K were considered.

In Fig. 6, the combined excitation–relaxation dynamics for various initial temperatures is studied. From the figure, which shows the expectation values of system energies, $\langle \hat{H}_s \rangle$, the following information can be drawn:

(1) Most importantly, also in this model the same qualitative temperature effects are observed as in Sect. 4.2.1: the relaxation proceeds the slower, the higher the temperature. Recurrences, if visible at all on the timescale of propagation, are shifted to longer times.
(2) Another temperature effect is that the maximum value of $\langle \hat{H}_s \rangle$ at $t \approx 1$ ps, i.e. the energy gain by IR excitation, increases slightly with increasing T. The larger energy gain can partially be explained by the

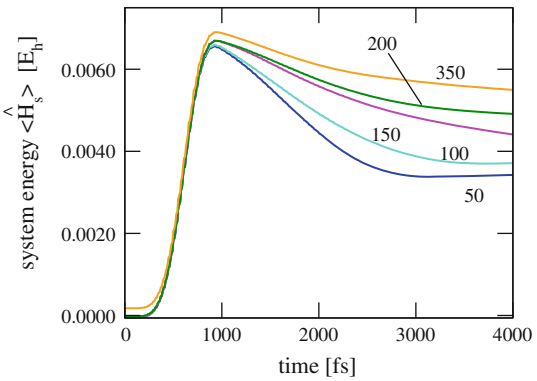

Fig. 6 Temperature dependence of the system energy after IR excitation with a 1 ps π-pulse. The numbers attached to the curves denote various temperatures in K

larger initial energy $\langle \hat{H}_s \rangle (t = 0)$ at higher temperatures, which is due to thermal excitation of higher-lying system levels. This argument holds true for $T = 350$ K only, however, and the higher maximum energy reached for $T = 200$ K, for example, must also have dynamical reasons.

Experimentally, the temperature-dependence of the relaxation of the ϕ-mode is not known. However, for the Si–H stretching mode it was found that the relaxation time *decreases* with increasing surface temperature [8]. This is also supported by theoretical work which makes use of Fermi's Golden Rule to calculate relaxation rates [4, 20, 21]: the relaxation (and thermal excitation) rates increase due to Bose–Einstein factors, which monotonically increase with temperature, i.e. lifetimes decrease. This is true not only for the stretching mode but for any mode, and in fact in Ref. [4] the opposite temperature effect for the bending mode has been predicted as here.

This "puzzle" may have many reasons. We stress that the choice of type and number of surface oscillators, and, to a smaller extent, also of the computational parameters (type of mode combination, number of SPFs and DVR points) has some influence on the results. However, in a systematic study on H:Si(100) we always found the same qualitiative temperature behaviour as described above. Furthermore, bath anharmonicities and/or bath–bath coupling terms, both of which were not considered in this work, may change the picture somewhat. First of all, however, it would be necessary to have lifetime measurements also for the bending mode in H:Si(100), at various temperatures to come up with a final conclusion. Finally, the role played by sample preparation and surface imperfections also for the Si–H stretching mode, has to be understood more thoroughly. At the moment it is only fair to say that within the present model the solution of the combined system–bath Schrödinger equation gives a qualitatively different picture than a Golden Rule, perturbative treatment [4]. Since it is known that vibrational relaxation can become faster or slower with temperature, depending on the system [22, 23], the perturbative, Golden-rule type approach appears to be too simple to explain temperature effects, while being often well suited for other purposes. It has been suggested in Ref. [22], that indeed the observed, complicated temperature dependence of vibrational lifetimes can result from the temperature-dependence of the phonon density of states and the coupling elements, which is not included in the Golden Rule.

5 Summary and outlook

The temperature dependence of the vibrational relaxation of the Si–Si–H bending mode in H:Si(100)(2 × 1) was investigated. A model was chosen which consists of a two-mode subsystem, describing the stretching and bending vibrations of a single H atom on a Si dimer, which was coupled to a set of 20 harmonic bath oscillators which represent the silicon surface and the remaining hydrogen atoms. For the solution of the combined system–bath Schrödinger equation, the MCTDH method was used. It was found that the vibration of the ϕ-mode has a "lifetime", or rather, a characteristic system–bath energy transfer time, of about 1 ps at 0 K, which agrees with previous investigation [4, 5]. The excitation by an IR laser pulse results in a mode- but not state-selective, excitation of the ϕ-mode. For two different scenarios, a "sudden excitation" and an "IR excitation" model, respectively the trend of longer lifetimes with increasing temperatures was found. The temperature dependence of the relaxation dynamics of the bending mode is experimentally unknown, but our findings are at variance with a perturbative model [4], and also with temperature-dependent measurements for the H–Si stretching mode of H:Si(100)(2 × 1) [8]. This may be due to shortcomings of the model or its numerical realization, but also on the experimental side further investigation appear to be necessary.

In conclusion, the explicit treatment of coupled system–bath problems, even with temperature and under the inclusion of external driving forces, such as lasers, is nowadays feasible. This coherent and unitary approach is an interesting alternative to reduced descriptions such as open-system density matrix theory, and may lead, as demonstrated here, to different conclusions. Of course, still only a limited number of bath modes can be included in realistic, unitary models, even when using MCTDH. However, recently approximations/extensions for MCTDH have been developed, such as the *local coherent state approximation* (LCSA) [19], or the *Gaussian MCTDH* (G-MCTDH) [24] to treat a huge number of bath modes.

Acknowledgments This paper is dedicated to the memory of Prof. Jürgen Hinze, who made important contributions to multi-configuration quantum methods, which also inspired this work. This work was supported by the Deutsche Forschungsgemeinschaft through project Sa 547/7-3.

References

1. Breuer H-P, Petruccione F (2002) The theory of open quantum systems. Oxford University Press, Oxford
2. May V, Kühn O (2000) Charge and energy transfer dynamics in molecular systems. Wiley, Berlin
3. Saalfrank P (2006) Chem Rev 106:4116
4. Andrianov I, Saalfrank P (2006) J Chem Phys 124:034710
5. Andrianov I, Saalfrank P (2006) Chem Phys Lett 433:91
6. Paramonov GK, Beyvers S, Andrianov I, Saalfrank P (2007) Phys Rev B 75:045405
7. Paramonov GK, Andrianov I, Saalfrank P (2007) J Phys Chem C 111:5432
8. Guyot-Sionnest P, Lin PH, Hiller EM (1995) J Chem Phys 102:4269
9. Liu Z, Feldman LC, Tolk NH, Zhang Z, Cohen PI (2006) Science 312:1024
10. Tully JC (2006) Science 312:1004
11. Meyer H-D, Manthe U, Cederbaum L (1990) Chem Phys Lett 165:73
12. Beck MH, Jäckle A, Worth GA, Meyer H-D (2000) Phys Rep 324:1
13. Gelman D, Kosloff R (2003) Chem Phys Lett 381:129
14. Nest M, Kosloff R (2007) J Chem Phys 127:134711
15. Nest M, Meyer H-D (2003) J Chem Phys 119:24
16. Colbert DT, Miller WH (1992) J Chem Phys 96:1982
17. Dyson AJ, Smith PV (1999) Mol Phys 96:1491
18. Sbraccia C, Silvestrelli PL, Ancilotto F (2002) Surf Sci 516:147
19. Martinazzo R, Nest M, Saalfrank P, Tantardini GF (2006) J Chem Phys 125:194102
20. Persson BNJ, Avouris P (1997) Surf Sci 390:45
21. Foley ET, Kam AF, Lyding JW, Avouris P (1998) Phys Rev Lett 80:1336
22. Tokmakoff A, Sauter B, Fayer MD (1994) J Chem Phys 100:9035
23. Kenkre VM, Tokmakoff A, Fayer MD (1994) J Chem Phys 101:10618
24. Burghardt I, Nest M, Worth GA (2003) J Chem Phys 119:5364